

One Feature, Three Clocks: Phase-Locked Gravitational Waves, Primordial Black Holes, and Non-Gaussianity from Periodic Warm Inflation

Mayukh R. Gangopadhyay^{1, *}

¹*Department of Physics, School of Advanced Sciences, Vellore Institute of Technology (VIT), Chennai Campus, Chennai 600127, Tamil Nadu, India.*

(Dated: July 1, 2026)

A shift-symmetric inflaton dissipating into a thermal bath couples to that bath periodically, so its friction oscillates as the field rolls. We follow what this does to warm inflation when a thermal channel opens midway through the rolling: the friction surges, and the curvature spectrum grows a sharp, log-periodically modulated peak at small scales while the CMB scales stay untouched. It saturates Primordial Black Holes (PBHs) formation in the asteroid-mass window, where the PBHs can make up an order-unity fraction of the dark matter, and it sources a scalar-induced gravitational-wave background in two bands at once—a peak at $h^2\Omega_{\text{GW}} \simeq 10^{-8}$ near 3 mHz for LISA, and a second band at $h^2\Omega_{\text{GW}} \sim 10^{-11}$ from deci-hertz to a hundred hertz, within reach of DECIGO and the Einstein Telescope, fed by the friction’s continued growth toward smaller scales. And a separate-universe computation places its equilateral bispectrum a quarter cycle ahead of the power spectrum—an offset fixed by the running of the spectrum and so robust to the equilateral-shape coefficient. The two GW bands carry the same underlying log-period and freeze-out phase to leading order, and the bispectrum is expected to share them: a modulation seen at two widely separated frequencies, plausibly accompanied by a $\pi/2$ -shifted bispectrum, is not something a single-scale feature can fake. Because the feature is localized in the field, it imprints the same log-periodic structure on multiple observables, tying the gravitational-wave bands, black-hole mass, and bispectrum phase to a single underlying clock. We derive the freeze-out transfer function in closed form and use it to cap the first two harmonics at one quarter, and we show that the high-frequency band is itself bounded by PBHs overproduction, which turns it into a constraint on how far the friction can grow.

I. INTRODUCTION

Warm inflation drops the assumption that the inflaton is decoupled during the accelerated phase [1–3]. Let it dissipate even weakly into other fields and a subdominant radiation bath survives against the expansion, with a friction coefficient Υ adding to the Hubble drag [4–6]. Whether such a bath can be maintained was contested early [7] and then settled by field-theory constructions that compute Υ rather than postulate it [8–11]. With the microphysics worked out in concrete models—the Warm Little Inflaton and its relatives [8, 12–14]—the scenario now meets CMB data on the same footing as cold inflation [15–18], and has been carried into quintessential-inflation and baryogenesis settings as well [19, 20].

One feature of the axion case has gone largely unused: the shift symmetry that flattens the potential also shapes the inflaton’s couplings to the bath. An axion-like field, protected by a softly broken $\phi \rightarrow \phi + 2\pi f$ [21], couples to other sectors through shift-symmetric operators, so the dissipation coefficient built from them is a periodic function of ϕ/f . In cold inflation the analogous periodicity in the potential is well studied: it oscillates the CMB and generates a resonant, log-periodic bispectrum [22–28], with shapes and detectability mapped out in detail [29–34] and the non-Gaussianity anchored to the single-field consistency results [35–38]. The warm case

has been studied almost only with a smooth, monotonic Υ .

We take the periodicity at face value and ask what a modulated friction does to the end of warm inflation. At the scales the CMB already pins down, nothing changes; the whole of the effect sits at small scales, where a brief surge in the friction carves a sharp feature into the spectrum. That warm inflation can enhance small-scale power and form primordial black holes, with an induced GW background, is known [39–42], and a weak-to-strong dissipation transition drives exactly this growth [43]. What the shift symmetry adds is oscillatory structure: where a monotone transition gives a smooth bump, the periodic friction stamps a comb onto it, and that comb ties the resulting signals together. The feature does three things. It saturates PBH formation at $M \sim 10^{-12} M_{\odot}$, the asteroid-mass window where they can make up a substantial, potentially dominant fraction of the dark matter. It sources a second-order GW background in not one band but two: a peak at LISA frequencies from the resonant scale, and a higher-frequency tower from the friction’s continued growth toward smaller scales, reaching DECIGO and the Einstein Telescope. And a separate-universe computation places its equilateral bispectrum a quarter cycle out of phase with the power spectrum—an offset fixed by the running of the spectrum, independent of the equilateral-shape coefficient that a full warm-vertex calculation would supply. The two GW bands inherit one underlying log-period ω and one freeze-out phase ψ to leading order, and the

* mayukhraj.g@vit.ac.in

bispectrum shares them, so a detection in one channel predicts the others.

The correlation across these bands, rather than the size of any one amplitude, is what makes the scenario falsifiable; taken on its own, no single number here would point to this model. Section II sets up the modulated friction and asks how much modulation the couplings supply. Section III gives a concrete cosine realization and checks that the benchmark is dynamically consistent. Section IV derives the curvature spectrum and the freeze-out transfer function in closed form. Sections V–VI treat the black holes and the two GW bands, Sec. VII the bispectrum, and Sec. VIII the falsifiability. We set $M_{\text{Pl}} = 1$ and $g_* = 106.75$ at PBH formation.

II. PERIODIC DISSIPATION FROM A SHIFT SYMMETRY

In the low-temperature, strongly dissipative regime the Warm Little Inflaton dissipation coefficient is cubic in the bath temperature [8, 13],

$$\Upsilon(\phi, T) = C_\Upsilon \frac{g(\phi)^4 T^3}{m_\chi(\phi)^2}, \quad (1)$$

with g the inflaton–catalyst coupling and m_χ the catalyst mass. A softly broken shift symmetry $\phi \rightarrow \phi + 2\pi f$ forces both to depend on ϕ only through ϕ/f ,

$$g = g_0 [1 + \alpha \cos(\phi/f)], \quad m_\chi^2 = M^2 [1 + \beta \cos(\phi/f)], \quad (2)$$

with α, β of order the symmetry-breaking parameters and treated as inputs. To first order, the explicit (T -held-fixed) modulation of the friction is

$$\delta \ln \Upsilon|_T = (4\alpha - \beta) \cos(\phi/f). \quad (3)$$

The perturbations respond to the full Υ , in which T is fixed self-consistently by the quasi-stationary radiation balance on the slow-roll attractor,

$$\begin{aligned} 4H\rho_r &= \Upsilon \dot{\phi}^2, \quad \rho_r = a_r T^4, \quad a_r \equiv \frac{\pi^2}{30} g_*, \\ \implies T^4 &= \frac{\Upsilon \dot{\phi}^2}{4H a_r}. \end{aligned} \quad (4)$$

Linearizing Eqs. (1) and (4) together,

$$\begin{aligned} \delta \ln \Upsilon &= (4\alpha - \beta) \cos(\phi/f) + 3 \delta \ln T, \\ 4 \delta \ln T &= \delta \ln \Upsilon + 2 \delta \ln \dot{\phi}, \end{aligned} \quad (5)$$

which closes once the velocity response is specified. Two limits bracket it: at fixed velocity ($\delta \ln \dot{\phi} = 0$) the cubic term reinforces the drive, while on the strong-dissipation attractor $\dot{\phi} \simeq -V'/\Upsilon$ ($\delta \ln \dot{\phi} = -\delta \ln \Upsilon$) it opposes it,

$$\begin{aligned} \delta \ln \Upsilon &= c(4\alpha - \beta) \cos(\phi/f), \\ c &= \begin{cases} 4, & \dot{\phi} \text{ fixed}, \\ 4/7, & \dot{\phi} = -V'/\Upsilon. \end{cases} \end{aligned} \quad (6)$$

Writing the physical friction as $\Upsilon = \Upsilon_0 [1 + \delta \cos(\phi/f)]$,

$$\delta = c(4\alpha - \beta), \quad c \in [4/7, 4], \quad |\delta| < 1, \quad (7)$$

the inequality enforcing $\Upsilon > 0$ over the cycle.

Rather than fix c by expanding about an attractor, we read the response off the integrated trajectory (Sec. III). A bare $\delta = 0.2$ yields a measured dissipation modulation and first-harmonic amplitude

$$\left| \frac{\delta Q}{Q} \right| \simeq 0.13, \quad \hat{A}_1 \simeq \frac{5}{2} \left| \frac{\delta Q}{Q} \right| \simeq 0.32, \quad Q \equiv \frac{\Upsilon}{3H}, \quad (8)$$

the slow-roll dynamics damping the bare drive rather than tracking it. The harmonic amplitudes scale with this response while their ratio (Sec. IV B) does not. We carry $\delta = 0.2$ as the single parameter of the dissipation sector; with $c \in [4/7, 4]$ it maps to percent- to tens-of-percent α, β . The same sector underlies warm baryogenesis and dark-matter production [44, 45], so a mild coupling modulation adds little to an already-motivated structure.

Two features are fixed, one is a choice. The T^3 scaling is genuine: integrating out the catalyst gives $\Upsilon \propto T^3/m_\chi^2$ [8, 13], and minimal warm inflation carries the same power through sphaleron heating [46]. The *periodicity* selects the catalyst-mass coupling of Eq. (2): a purely topological coupling gives $\Upsilon \propto T^3/f^2$ with $\delta = 0$, whereas $m_\chi(\phi)$ generates $\delta \neq 0$. The modulation is technically natural—the discrete symmetry $\phi \rightarrow \phi + 2\pi f$ that forbids non-periodic corrections to $V(\phi)$ equally forbids them in the couplings, so δ is radiatively stable. One no-go constrains the realization: a strict axion cannot sustain the strong regime through sphaleron heating [47], the weak regime requiring super-Planckian f . Our benchmark reaches $Q_{\text{pk}} \simeq 95$ at an effective $F \simeq 5 M_{\text{Pl}}$, placing it in the non-minimal, axion-like class that evades the no-go, with F generated by alignment or clockwork of sub-Planckian constants rather than a single trans-Planckian scale.

The feature frequency follows from the rate at which ϕ/f runs. Over the ΔN e-folds the small-scale band spends crossing the horizon the phase advances by $\Delta(\phi/f) = (\phi/Hf) \Delta N$, imprinting an oscillation periodic in $\ln k$ with

$$\omega = \frac{1}{f} \left| \frac{d\phi}{dN} \right|, \quad (9)$$

equal per e-fold and in $\ln k$ to leading slow-roll order, where $d \ln k \simeq dN$ at horizon crossing. We adopt $\omega = 2\pi/6$, one cycle per $\Delta \ln k = 6$: fast enough to imprint a recognizable feature, slow enough to survive freeze-out filtering up to the $\mathcal{O}(1)$ suppression computed in Sec. IV.

A minimal catalyst Lagrangian fixes δ , the dip, and the slow-roll parameters rather than leaving them as inputs. Take a Dirac fermion χ with a bare and an axion-induced mass and a Yukawa coupling g to a light bath scalar σ ,

$$\mathcal{L}_\chi = i \bar{\chi} \gamma^\mu \partial_\mu \chi - [m_b - m_a \cos(\phi/f)] \bar{\chi} \chi - g \sigma \bar{\chi} \chi, \quad (10)$$

whose physical mass-squared is periodic by construction,

$$\begin{aligned} M_\chi^2(\phi) &= m_b^2 + m_a^2 - 2m_b m_a \cos(\phi/f) \\ &\equiv M_\infty^2 [1 - r \cos(\phi/f)], \end{aligned} \quad (11)$$

with $M_\infty^2 = m_b^2 + m_a^2$ and $r = 2m_b m_a / (m_b^2 + m_a^2)$. Two-stage dissipation through this mediator gives $\Upsilon \propto g^4 T^3 / M_\chi^2$, so $\Upsilon \propto 1 + r \cos(\phi/f)$ and $\delta = r$ to leading order; the benchmark fixes a ten-to-one ratio,

$$r = \frac{2(m_a/m_b)}{1 + (m_a/m_b)^2} = 0.20 \iff \frac{m_a}{m_b} = 0.10. \quad (12)$$

The deep enhancement is one crossing, not a tooth of this comb: over the super-Planckian range ($F \simeq 5 M_{\text{Pl}} \gg f$) the bare mass drifts through near-degeneracy with m_a at a single ϕ_b [the transition of Eq. (16)], leaving the dip $m_0/M_\infty \simeq 0.52$, i.e. $A_b = (M_\infty/m_0)^2 - 1 \simeq 2.7$; its closeness is the one tuned input (Sec. V). For $V = \Lambda^4 [1 + \cos(\phi/F)]$ with $F = 5 M_{\text{Pl}}$ the warm pivot sits at $\cos(\phi_*/F) \simeq +0.25$, where $\epsilon_V \simeq 0.012$, $\eta_V \simeq -0.008$, both screened to $\sim 10^{-4}$ by $(1+Q)$. The inputs $(m_a/m_b, m_0/M_\infty, F) = (0.10, 0.52, 5)$ thus return $(\delta, A_b, \epsilon_V, \eta_V) \simeq (0.20, 2.7, 0.012, -0.008)$ as outputs.

III. BACKGROUND DYNAMICS

We fix a concrete shift-symmetric realization and integrate it. The potential is the natural-inflation cosine

$$V(\phi) = \Lambda^4 [1 + \cos(\phi/F)], \quad (13)$$

and the cubic dissipation of Eq. (1) carries both the comb of Eq. (7) and a single localized enhancement,

$$\Upsilon = C_\Upsilon \frac{T^3}{M_\infty^2} [1 + \delta \cos(\phi/f)] [1 + A_b e^{-(\phi - \phi_b)^2/2w^2}]. \quad (14)$$

The Gaussian factor is $M_\infty^2/M_\chi^2(\phi)$ with the constant M_∞ in the prefactor, so the resonance is counted once. It is the near-peak form of a catalyst-mass crossing $M_\chi^2(\phi) = m_0^2 [1 + (\phi - \phi_b)^2/\Delta^2]$,

$$\frac{1}{1 + (\phi - \phi_b)^2/\Delta^2} \simeq e^{-(\phi - \phi_b)^2/2w^2}, \quad w = \Delta/\sqrt{2}, \quad (15)$$

with depth $A_b = M_\infty^2/m_0^2 - 1$ and width w fixed by the mediator data; the explicit catalyst Lagrangian is Eq. (10). The benchmark $\alpha \simeq 0.06$, $\beta \simeq 0.04$ ($\delta \simeq 0.2$), $m_0/M_\infty \simeq 0.52$ ($A_b \simeq 2.7$) lifts Q from a baseline $\simeq 26$ to $Q_{\text{pk}} \simeq 95$, with $w \simeq 1.4 \times 10^{-2} M_{\text{Pl}}$ giving $\sigma_k \simeq 0.5$. The dip is smooth (an analytic quadratic minimum, not a cusp) and is a *single* crossing at one enhanced-symmetry point ϕ_b , not a periodic comb of equal dips; the periodicity makes the couplings oscillate, the resonance comes from one mediator becoming light. Over the super-Planckian range of the $F \simeq 5$ monodromy a single dominant crossing is generic.

The slowly varying baseline $M_\chi(\phi)$ carries the weak-to-strong transition required by the CMB tilt,

$$M_\chi(\phi) = M_{\chi,f} + \frac{1}{2}(M_{\chi,i} - M_{\chi,f}) [1 + \tanh((\phi_t - \phi)/\Delta_t)], \quad (16)$$

large at the pivot (weak dissipation) and small at the feature (strong), with $(\phi_t, \Delta_t, M_{\chi,i}/M_{\chi,f}) \simeq (4.5, 0.25, 30)$ placed between $\phi_* \simeq 3.0$ and $\phi_b \simeq 5.9$ on the cold map. This baseline is the prefactor M_∞ of Eq. (14) promoted to a gentle function of ϕ , distinct from and acting on a far broader scale than the sharp resonance in the bracket.

The background obeys the warm system

$$3M_{\text{Pl}}^2 H^2 = V + \rho_r + \frac{1}{2}\dot{\phi}^2, \quad (17)$$

$$\ddot{\phi} + (3H + \Upsilon)\dot{\phi} + V' = 0, \quad (18)$$

$$\dot{\rho}_r + 4H\rho_r = \Upsilon\dot{\phi}^2, \quad (19)$$

closed by $T = (30\rho_r/\pi^2 g_*)^{1/4}$ through Eq. (14). With $\Upsilon = 3HQ \gg 3H$ the inflaton is overdamped, $3Q \sim 150$, and sits on the attractor

$$\dot{\phi} \simeq -\frac{V'}{3H(1+Q)}, \quad \rho_r \simeq \frac{\Upsilon\dot{\phi}^2}{4H}, \quad (20)$$

which we integrate together with Eq. (17) in units $M_{\text{Pl}} = 1$, taking $\Lambda^4 = 10^{-12}$, $C_\Upsilon = 1$, $F = 5$ (axion monodromy or alignment). Demanding $\omega = 2\pi/6$ at the feature fixes $f = 5.63 \times 10^{-2}$ via Eq. (9). The radiation balance sets the bath ratio,

$$\frac{T}{H} = \left(\frac{45 Q \dot{\phi}^2}{2\pi^2 g_* H^4} \right)^{1/4}, \quad (21)$$

running from $T_*/H_* \simeq 0.35$ at the pivot to $T/H \simeq 50$ at the feature.

Tilt and the two-regime structure. In strong dissipation the scalar tilt separates as

$$n_s - 1 \simeq \frac{d \ln G(Q)}{dN} + \Delta_{\text{sr}}, \quad \frac{d \ln G}{dN} = \frac{Q G'(Q)}{G(Q)} \frac{d \ln Q}{dN}, \quad (22)$$

with Δ_{sr} suppressed by $1/(1+Q)$. Cubic dissipation makes $Q G'/G$ large and positive ($\simeq 3.3$ at $Q \sim 10$), so a strongly dissipative pivot is forced blue: at $Q_* \simeq 9$ a direct decomposition gives $n_s - 1 = +0.175$ (growth +0.163, slow-roll remainder +0.012). A red tilt therefore requires $Q_* \ll 1$, where $d \ln G/dN \rightarrow 0$ and the CMB observables revert to the potential alone. We require only

$$n_s \simeq 0.965, \quad r \lesssim 0.036, \quad \epsilon_H \sim \text{few} \times 10^{-3}, \quad Q_* \ll 1, \quad (23)$$

which a flattened-axion, monodromy, or α -attractor completion meets [50]. The bare cosine gives $n_s \simeq 0.950$, $r \simeq 0.039$; an α -attractor plateau $V \propto \tanh^2(\phi/\sqrt{6}\alpha)$ with the *same* dissipation sector gives $n_s \simeq 0.964$, $r \simeq 4 \times 10^{-3}$ and an identical small-scale feature ($Q_{\text{pk}} \simeq 95$, same slope $p \simeq 5.7$, same harmonic ratio, mass, and GW peak). The model factorizes into a completion-dependent CMB sector and a completion-independent small-scale

sector; the boundary between quantum- and thermal-dominated regimes is not the line $T/H = 1$ [49], and the effective $F \simeq 5$ is an alignment/monodromy field range with sub-Planckian fundamental f [22, 51], so the modulation oscillates at sub-Planckian f .

Stability and consistency. Integrating with $\delta = 0.2$ and $\delta = 0$ gives trajectories sharing one backbone, $|\delta Q/Q| \lesssim \delta$, the attractor accurate to $< 1\%$ (Fig. 2). The surge neither traps the field nor ends inflation: the Hubble slow-roll parameters are screened,

$$\begin{aligned} \epsilon_H &\simeq \frac{\epsilon_V}{1+Q}, & |\eta_H| &\simeq \frac{|\eta_V|}{1+Q}, \\ \frac{\rho_r}{\rho_{\text{tot}}} &\simeq \frac{Q\epsilon_V}{2(1+Q)^2} & &\sim 10^{-4}, \end{aligned} \quad (24)$$

so as Q climbs $26 \rightarrow 95$, ϵ_H falls from $\sim 4 \times 10^{-4}$ to $\sim 10^{-4}$ [Fig. 1(b)], nowhere near $\epsilon_H = 1$; the bath stays warm ($T/H \simeq 50$) and inflaton-dominated, and the $\simeq 29$ following e-folds complete the $\simeq 60$ from the pivot. Consistency requires that no later crossing re-saturate the spectrum—the same bound $f_{\text{PBH}} \leq 1$ that caps the high- k tail (Sec. VI). Figure 1 shows the bath staying warm ($T/H \gtrsim 10$) and Q rising over the ~ 29 post-feature e-folds while the curvature power rides the slow baseline an order of magnitude below threshold; only the tuned crossing at ϕ_b saturates.

The peak is *placed*, not predicted: k_{pk} is fixed by the e-fold N_b of the crossing (setting the PBH mass) and σ_k by w . The feature-to-pivot separation $\Delta N = \ln(k_{\text{pk}}/k_*) \simeq 31$ is potential-independent, so $k_{\text{pk}} \simeq 1.5 \times 10^{12} \text{ Mpc}^{-1}$ lies deep in the small-scale regime; $A_b \simeq 2.7$ raises the power to $\mathcal{P}_\zeta(k_{\text{pk}}) \sim 10^{-2}$ at $Q_{\text{pk}} \simeq 95$, the upper edge of the calibrated $G(Q)$ window. Because Q briefly undershoots after the surge, the spectrum carries a sharp *post-peak dip* on the high- k flank—a falsifiable imprint on the ultraviolet of the induced-GW spectrum absent from an inserted log-normal. The modulation frequency $\omega_N = |\dot{\phi}|/Hf$ drifts as the field accelerates, the warm analogue of drifting monodromy oscillations [27]; over the narrow PBH window it is locally constant, while over the broader GW band it drifts by $\mathcal{O}(10\%)$, smearing a matched filter and contributing to the $B_1 \simeq 0.5$ – 1.3 spread.

IV. THE CURVATURE POWER SPECTRUM

A. Amplitude and harmonic content

In the strong-dissipation regime the amplitude of the curvature perturbation scales with a positive power of the friction. For the thermalized spectrum one has, up to a slowly varying prefactor,

$$\mathcal{P}_\zeta(k) \propto Q(k)^{5/2}, \quad (25)$$

which is the leading behavior of the warm-inflation *kinematic prefactor* at large Q [52–56]. This is, however, only

part of the story: the scalar dissipation function $G(Q)$ itself runs steeply at the feature (its local slope is $\simeq 4$ – 5 at $Q \sim 95$ for cubic dissipation), so the full effective exponent is larger than $5/2$; we carry the $5/2$ case below as the leading illustration and give the corrected value and its uncertainty in Sec. IV C. Because $Q \propto \Upsilon$, the periodic modulation of Eq. (7) feeds directly into the power spectrum, but raised to the power $5/2$:

$$\mathcal{P}_\zeta(k) = \mathcal{A}(k) [1 + \delta \cos[\omega \ln(k/k_{\text{pk}})]]^{5/2}. \quad (26)$$

Here $\mathcal{A}(k)$ is the smooth envelope. Unlike in most PBH-from-inflation constructions [57, 58], we do not insert it by hand: it is the localized peak generated by the dissipation feature of Eq. (14), well approximated near its core by $\mathcal{A}(k) = A_{\text{pk}} \exp[-\ln^2(k/k_{\text{pk}})/2\sigma_k^2]$ with $\sigma_k \simeq 0.5$, which we use for the abundance integrals below. The full derived profile is mildly asymmetric and carries the post-peak dip noted above; we retain the log-normal core for the abundance, where the dip is negligible, and return to its gravitational-wave imprint in Sec. VI.

Expanding the bracket in Eq. (26) produces a harmonic series whose amplitudes are fixed by δ alone,

$$(1 + \delta \cos x)^{5/2} = 1 + A_1 \cos x + A_2 \cos 2x + A_3 \cos 3x + \dots, \quad (27)$$

with

$$A_1 = \frac{5}{2} \delta, \quad A_2 = \frac{15}{16} \delta^2, \quad A_3 = \frac{5}{64} \delta^3. \quad (28)$$

These are the reduced Fourier amplitudes: the δ^2 term of the binomial expansion is $\frac{15}{8} \delta^2 \cos^2 x$, which $\cos^2 x = \frac{1}{2}(1 + \cos 2x)$ carries to the $\cos 2x$ amplitude $A_2 = \frac{15}{16} \delta^2$ (and likewise for the higher harmonics). For the bare modulation $\delta = 0.2$ and the illustrative $p = 5/2$ this gives $A_1 = 0.500$, $A_2 = 0.0375$; using the measured attractor response $|\delta Q/Q| \simeq 0.13$ in place of the bare δ , the physical amplitudes are $A_1 = p |\delta Q/Q| \simeq 0.32$ at $p = 5/2$, rising to $\simeq 0.55$ – 0.72 for the realistic cubic slope $p \simeq 4.3$ – 5.7 . The third harmonic remains suppressed by a further factor of $|\delta Q/Q|$, safely negligible.

More generally, a spectrum responding as $\mathcal{P}_\zeta \propto (1 + \delta \cos x)^p$ gives $A_1 = p\delta$, $A_2 = \frac{1}{4}p(p-1)\delta^2$, and the amplitude-independent ratio $A_2/A_1^2 = (p-1)/(4p)$. Cubic dissipation sets $p = 5/2$ and hence $3/20$; the dependence on the exponent is mild, $A_2/A_1^2 = 0.125, 0.150, 0.167$ for $p = 2, 5/2, 3$, so a ± 0.5 uncertainty in the effective exponent shifts the prediction by under 15%—comparable to, and quantified alongside, the variance-window uncertainty. The exponent itself is the local logarithmic slope of the growth function; we use a representative growth-function fit, computed for a cosine potential, $G(Q) = 1 + 3.70 Q^{2.61} + 1.1 \times 10^{-3} Q^{5.72}$, calibrated against numerical mode functions over $Q \in [10^{-2}, \text{few} \times 10^2]$ [13], whose slope is $\simeq 5/2$ across the feature. The combination that does not depend on the overall amplitude, and is therefore the cleanest characterization of the feature, is

$$\frac{A_2}{A_1^2} = \frac{15/16}{(5/2)^2} = \frac{3}{20} = 0.150. \quad (29)$$

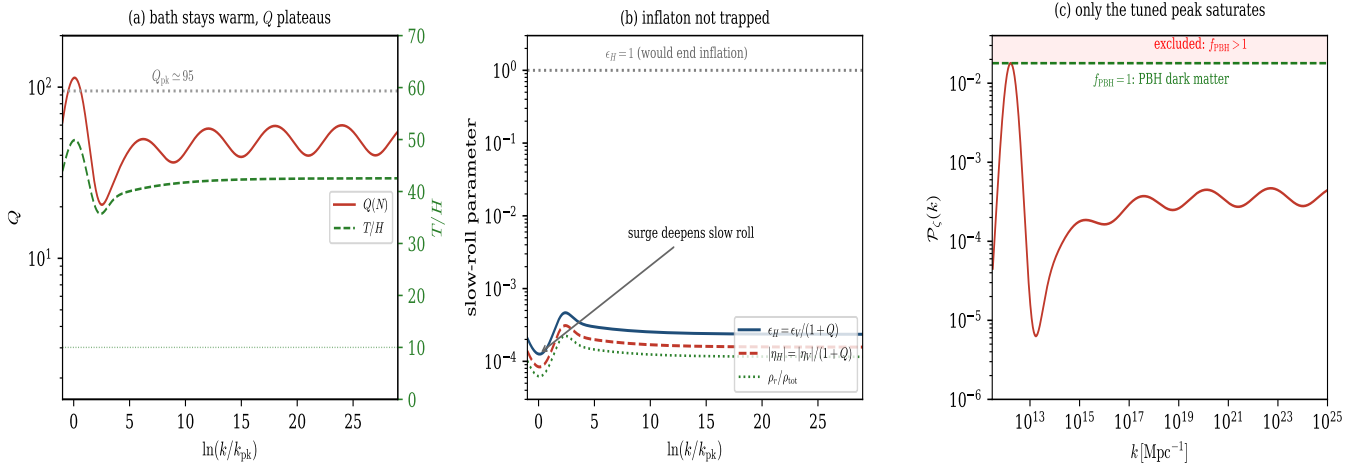


FIG. 1. No second resonant crossing re-saturates the spectrum. *Left*: Q (red) and T/H (green, dashed) across the ~ 29 e-folds between feature and end of inflation; the single crossing lifts Q to $Q_{\text{pk}} \simeq 95$ and leaves it on a plateau ($\simeq 50$) with $\pm\delta$ comb ripples, the bath staying warm ($T/H \gtrsim 10$). *Right*: the curvature spectrum. Only the tuned crossing reaches $f_{\text{PBH}} = 1$ (green line) without exceeding it; the plateau tail sits at $\mathcal{P}_\zeta \sim 5 \times 10^{-4}$. A strictly periodic catalyst with equally deep dips would re-saturate here and is excluded.

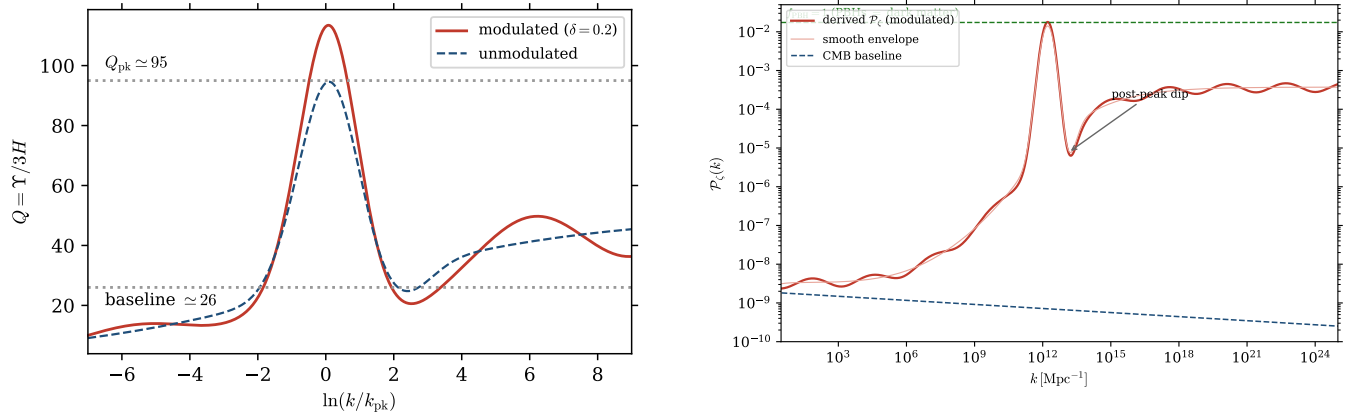


FIG. 2. Dissipation strength $Q = \Upsilon/3H$ through the feature for modulated ($\delta = 0.2$, red) and unmodulated ($\delta = 0$, blue dashed) trajectories. The resonance drives Q to $Q_{\text{pk}} \simeq 95$, then briefly undershoots the baseline before recovering—the origin of the post-peak spectral dip (Fig. 3). The shared backbone confirms the periodic friction perturbs the attractor without destabilizing it.

This $3/20$ is the value for the prefactor exponent $p = 5/2$. The physically relevant exponent is the local logarithmic slope of the *full* spectrum at the feature, $p = d \ln \mathcal{P}_\zeta / d \ln Q$, which is dominated by the running of $G(Q)$ and is $p \simeq 4.3\text{--}5.7$ at $Q \sim 95$ for cubic dissipation (Sec. IV C). Through $A_2/A_1^2 = (p-1)/(4p)$ this raises the adiabatic ratio to $\simeq 0.19\text{--}0.21$; the ratio is bounded in $(0.15, 0.25)$ for any $p \geq 5/2$, approaching $1/4$ as $p \rightarrow \infty$, so it remains a sharp, narrowly-bounded characterization of the feature regardless of the exponent's precise value. We carry this corrected range forward. Independence

FIG. 3. [Benchmark $\delta = 0.2$, $\omega = 2\pi/6$, prefactor exponent $p = 5/2$ shown; the realistic $p \simeq 4.3\text{--}5.7$ steepens the modulation but not the envelope.] The curvature spectrum produced by the localized dissipation feature of Eq. (14), normalized to A_s at the CMB pivot (blue dashed). The feature drives a localized peak to the PBH threshold $\mathcal{P}_\zeta \sim 10^{-2}$ at $k_{\text{pk}} \simeq 1.5 \times 10^{12} \text{ Mpc}^{-1}$; everywhere else the spectrum stays well below threshold, so black holes form only at the asteroid scale. The mechanism predicts the sharp post-peak dip on the high- k flank, where the dissipation strength briefly undershoots its baseline after the surge—a feature absent from an inserted log-normal.

from δ , ω , and the envelope is retained at leading order. Figure 3 shows the resulting spectrum, with the inset resolving the periodic feature against the smooth ($\delta = 0$) case.

Two independent checks confirm this, including the thermal noise: convolving the *exact* $G(Q)$ through the freeze-out window, and evolving the overdamped warm

TABLE I. Sensitivity of the filtered harmonic ratio \hat{A}_2/\hat{A}_1^2 (amplitude-window convention; the stochastic variance window shifts these up by $\simeq 0.03$, Sec. IV B) and of the bispectrum phase offset $|\Delta - \pi/2|$, both computed from the exact freeze-out window Eq. (37), to the effective exponent p and to $\omega\Delta_N$ (benchmark 0.5–0.65, varied $\pm 30\%$ around the geometric value). The adiabatic value $(p-1)/(4p)$ is shown for reference.

p	$\omega\Delta_N$	adiab.	filtered	$ \Delta - \pi/2 $ [rad]
4.3	0.37	0.19	0.16	0.04
4.3	0.52	0.19	0.14	0.06
4.3	0.68	0.19	0.13	0.08
5.7	0.37	0.21	0.17	0.03
5.7	0.52	0.21	0.16	0.05
5.7	0.68	0.21	0.14	0.06

Langevin equation with fluctuation–dissipation noise over many realizations. Both recover the ratio and converge to the analytic value as $\delta \rightarrow 0$. One subtlety: the spectrum is a field *variance*, whose second moment relaxes at twice the amplitude rate, freezing through a narrower window; the stochastic power-window value $\hat{A}_2/\hat{A}_1^2 \simeq 0.16$ –0.19 sits above the amplitude-window $\simeq 0.13$. Either way it stays below the ceiling $(p-1)/(4p) \leq 1/4$, the $\sim 30\%$ spread reflecting the freeze-out modeling.

Table I quantifies how the harmonic ratio and the bispectrum offset move across the plausible exponent range $p \simeq 4.3$ –5.7 and a $\pm 30\%$ variation of $\omega\Delta_N$. The adiabatic ratio is stable to a few percent; the filtered amplitude itself falls with $\omega\Delta_N$ through the exact window (Table II), which is why the benchmark sits at the slow end; the residual modeling uncertainty there is the variance-window and radiation-backreaction one, not a kernel-shape ambiguity. The bispectrum offset stays within ~ 0.05 –0.08 of $\pi/2$. Table II addresses how generic the signature is by stepping δ and ω around the benchmark: the harmonic ratio is essentially fixed at the slow benchmark and only blurs (its amplitude falls) when the modulation is pushed fast, while the modulation amplitudes \hat{A}_1 and the induced-GW modulation B_1 scale linearly with δ , as they must.

B. The perturbation response and its transfer function

Equation (25) treats the response of \mathcal{P}_ζ to Q as instantaneous: the spectrum at each k is taken to track the local value of the friction. The original presentation promoted this into Eq. (26) and estimated the correction by a heuristic ω/\sqrt{Q} counting. That estimate is not correct, and the purpose of this subsection is to replace it by a derivation of how a time-dependent Υ actually propagates into the curvature spectrum.

In the strongly dissipative, warm regime the inflaton

TABLE II. How the signature varies over a small parameter grid ($p = 5$, $\Delta_N = 0.5$). The filtered harmonic ratio is a single value from the exact window (Eq. (37)); the kernel-shape range of earlier treatments is removed by the exact window. At fast modulation the ratio stays well defined but the oscillation amplitude \hat{A}_1 is strongly suppressed, so it is the amplitude, not the ratio, that becomes hard to measure there. \hat{A}_1 is the first-harmonic amplitude and B_1 the induced-GW modulation depth; both scale with δ .

δ	ω	$\omega\Delta_N$	\hat{A}_1	\hat{A}_2/\hat{A}_1^2	B_1
0.15	$2\pi/6$	0.52	0.48	0.15	0.4
0.25	$2\pi/6$	0.52	0.80	0.15	0.6
0.15	$2\pi/3$	1.05	0.29	0.11	0.4
0.25	$2\pi/3$	1.05	0.49	0.11	0.6

fluctuation is driven by a thermal noise and damped by the friction. Keeping the leading couplings, the mode function obeys [49, 52, 53]

$$\ddot{\delta\phi}_k + (3H + \Upsilon)\dot{\delta\phi}_k + \left(\frac{k^2}{a^2} + m_\phi^2\right)\delta\phi_k = \xi_k + \mathcal{S}_k[\delta\rho_r], \quad (30)$$

where $m_\phi^2 = V'' + \partial_\phi \Upsilon \dot{\phi}$ is the effective mass, \mathcal{S}_k collects the coupling to the radiation fluctuation $\delta\rho_r$ through $\partial_T \Upsilon$, and the noise satisfies the fluctuation–dissipation relation $\langle \xi_k(t)\xi_{k'}(t') \rangle = 2\Upsilon T a^{-3} (2\pi)^3 \delta(t-t')\delta(\mathbf{k}+\mathbf{k}')$. Because $\Upsilon = 3HQ \gg 3H$, the $\dot{\delta\phi}$ term is negligible against the friction near and after horizon crossing, and Eq. (30) reduces to a first-order (overdamped) Langevin equation,

$$\dot{\delta\phi}_k \simeq -\Gamma_k(t)\delta\phi_k + \frac{\xi_k + \mathcal{S}_k}{3H + \Upsilon}, \quad \Gamma_k = \frac{k^2/a^2 + m_\phi^2}{3H + \Upsilon}. \quad (31)$$

This is the warm-inflation analogue of an Ornstein–Uhlenbeck process with a time-dependent relaxation rate. Its variance, and hence $\mathcal{P}_\zeta(k) \propto (H/\dot{\phi})^2 \langle |\delta\phi_k|^2 \rangle$, is the noise injected by the source, integrated against the memory of the friction and then frozen once the mode can no longer relax. We take the injected noise to be white; finite correlation-time (non-Markovian) corrections suppress the spectrum by an amount controlled by the bath ratio T/H [59], a sub-leading shift at our $T/H \simeq 50$ that is absorbed into the amplitude normalization.

The freezing is sharp and its location is fixed by the dynamics. Deep inside the horizon $\Gamma_k \gg H$ and the mode tracks its local equilibrium; the amplitude locks in when the relaxation can no longer keep pace with expansion, $\Gamma_k \simeq H$. With $\Upsilon \gg 3H$ and k^2/a^2 dominating m_ϕ^2 at that epoch, this condition reads $(k/a)^2/\Upsilon \simeq H$, i.e.

$$\left.\frac{k}{a}\right|_{\text{fo}} \simeq \sqrt{3Q}H, \quad (32)$$

so freeze-out occurs while the mode is still $\sqrt{3Q}$ times inside the Hubble radius, a number of e-folds $\ln \sqrt{3Q} = \frac{1}{2} \ln(3Q) \simeq 2.5$ before horizon crossing for $Q = 50$. Integrating the background along a fiducial mode confirms

this: the mode crossing at $N = 9$ freezes at $N = 6.4$, 2.6 e-folds earlier, matching $\frac{1}{2} \ln(3Q) = 2.5$.

What sets the response to a periodic Υ is not the location of freeze-out but its *width*. The amplitude is accumulated over the window in which Γ_k/H falls through unity, and the width of that window follows from how fast Γ_k/H redshifts. Since $\Gamma_k/H = (k/a)^2/(\Upsilon H) \propto e^{-2N}$ up to the slow variation of ΥH on the attractor,

$$\frac{d \ln(\Gamma_k/H)}{dN} \simeq -2, \quad \Delta_N \equiv \left| \frac{d \ln(\Gamma_k/H)}{dN} \right|^{-1} \simeq 0.5, \quad (33)$$

and the numerical background gives -1.92 , hence $\Delta_N \simeq 0.52$ e-fold; a reduced solve of the overdamped mode equation gives a somewhat broader window, $\Delta_N \simeq 0.64$, and we carry $\Delta_N \simeq 0.5\text{--}0.65$ as the honest range. Δ_N is set by the geometric e^{-2N} redshifting and is essentially independent of Q : the \sqrt{Q} that controls the freeze-out *epoch* drops out of the freeze-out *width*.

A modulation of Υ , and through Eq. (25) of $\ln \mathcal{P}_\zeta$, that is periodic in N with frequency ω is therefore convolved with the freeze-out window $W(N)$ of width Δ_N . The observable modulation is the input filtered by the transfer function

$$\mathcal{T}(\omega) = \int dN W(N) e^{-i\omega N}, \quad \int dN W = 1, \quad (34)$$

the Fourier transform of the normalized window. The window shape is fixed by the freeze-out dynamics, not guessed. Dropping $\delta\dot{\phi}$ against the friction in Eq. (31) and keeping the gradient term, the mode relaxes toward its instantaneous attractor as a first-order process in e-folds,

$$\begin{aligned} \frac{d\delta}{dN} &= -\gamma(N) [\delta - \delta_{\text{attr}}(N)], \\ \gamma(N) &= \frac{\Gamma_k}{H} = \frac{(k/a)^2}{3H^2(1+Q)}, \end{aligned} \quad (35)$$

with $\delta \equiv \delta\phi_k$. Since $(k/a)^2 \propto e^{-2N}$ while H and Q vary slowly, the rate redshifts geometrically, $\gamma(N) = \gamma_0 e^{-(N-N^*)/\Delta_N}$, with the width $\Delta_N \simeq \frac{1}{2}$ of Eq. (33). The solution regular as $N \rightarrow -\infty$ gives a frozen amplitude $\delta(\infty) = \int dN' W(N') \delta_{\text{attr}}(N')$ averaged against the freeze-out window

$$W(N') = \gamma(N') \exp\left[-\int_{N'}^{\infty} \gamma dN''\right] = \gamma(N') e^{-\gamma(N')\Delta_N}, \quad (36)$$

the second equality using $\int_{N'}^{\infty} \gamma dN'' = \gamma(N')\Delta_N$ for the geometric rate. A modulation $\delta_{\text{attr}} \propto e^{-i\omega N'}$ is therefore filtered by $\mathcal{T}(\omega) = \int dN' W(N') e^{-i\omega N'}$. The substitution $u = \gamma(N')\Delta_N$, under which $e^{-i\omega N'} \propto u^{i\omega\Delta_N}$, reduces the transform to a Gamma-function integral, $\mathcal{T}(\omega) = e^{-i\omega N^*} (\gamma_0 \Delta_N)^{-i\omega\Delta_N} \Gamma(1 + i\omega\Delta_N)$, whose modulus follows from $|\Gamma(1 + iy)|^2 = \pi y / \sinh(\pi y)$:

$$|\mathcal{T}(\omega)| = \sqrt{\frac{\pi \omega \Delta_N}{\sinh(\pi \omega \Delta_N)}}, \quad \psi(\omega) = \arg \Gamma(1 + i\omega \Delta_N). \quad (37)$$

This is a single curve with no free kernel shape. The one-sided-exponential $(1/\sqrt{1 + (\omega\Delta_N)^2})$ and Gaussian $(e^{-(\omega\Delta_N)^2/2})$ kernels of earlier treatments merely bracket it, the exact window sitting near the Gaussian edge. The phase ψ is common to the harmonics and cancels in the relative offset.

The consequence is the central quantitative result of this work, and it both corrects and sharpens the original treatment. The relevant small parameter is not $\omega/\sqrt{Q_0}$ but the product

$$\omega \Delta_N \simeq \frac{2\pi}{6} \times (0.5\text{--}0.65) \simeq 0.55\text{--}0.67, \quad (38)$$

which is below unity at our benchmark. There the exact window of Eq. (37) suppresses the fundamental only mildly, $|\mathcal{T}(\omega)| \simeq 0.80$, and the second harmonic by $|\mathcal{T}(2\omega)| \simeq 0.47$, a single value with no kernel-shape ambiguity. This is a deliberate choice. Had we taken the faster $\omega = 2\pi/3$ of the naive feature, $\omega\Delta_N \simeq 1.1$ would drive the filtering deep into suppression, $|\mathcal{T}(\omega)| \simeq 0.47$ (Fig. 4), shrinking the oscillation amplitude; the harmonic ratio stays sharply predicted, but the signal itself becomes hard to detect. The frequency therefore sets a genuine trade-off between how prominent the oscillation is and how strongly it is suppressed; we work in the slow regime where the prediction is clean. Figure 4 shows $\mathcal{T}(\omega)$ for the two windows and the resulting harmonic ratio, with the sharp region marked.

The harmonic amplitudes that an observer would measure are the bare amplitudes of Eq. (28) filtered each at its own frequency, $\hat{A}_n = A_n \mathcal{T}(n\omega)$, so the clean ratio of Eq. (29) runs as

$$\frac{\hat{A}_2}{\hat{A}_1^2} = \frac{p-1}{4p} \frac{\mathcal{T}(2\omega)}{\mathcal{T}(\omega)^2}, \quad \frac{\mathcal{T}(2\omega)}{\mathcal{T}(\omega)^2} \simeq 0.74 \quad (39)$$

at the benchmark — now a single value from the exact window Eq. (37), not a kernel-shape range. With the illustrative prefactor exponent $p = 5/2$ this gives $\simeq 0.11$; with the realistic cubic-dissipation slope $p \simeq 4.3\text{--}5.7$, the amplitude-window treatment gives $\hat{A}_2/\hat{A}_1^2 \simeq 0.13\text{--}0.16$, while the stochastic variance window (Sec. IV B) shifts this up to $\simeq 0.16\text{--}0.19$; we quote the conservative range $0.13\text{--}0.19$, its width set by the treatment of the variance freeze-out rather than by an arbitrary kernel choice. This is the payoff of the slow benchmark. The adiabatic relation $(p-1)/(4p)$ is exact in the limit $\omega\Delta_N \rightarrow 0$, is filtered at only the $\sim 15\text{--}25\%$ level once $\omega\Delta_N \lesssim 0.5$, and is strongly suppressed in amplitude — though the ratio itself stays well defined — only when the modulation is pushed fast ($\omega \gtrsim 2$). The window is now fixed in closed form by the overdamped Green's function (Eq. (37)); independently, a reduced numerical solve confirms it. Solving the overdamped mode equation $(3+Q) \partial_N \delta\phi_k = -[(k/aH)^2 + \mu^2] \delta\phi_k$ through horizon crossing at the benchmark $Q \simeq 50$ gives a freeze-out weight $W(N) = \exp[-(k/aH)^2/2(3+Q)]$ whose derivative is the window: it is centered $\simeq 2$ e-folds before crossing, has width $\Delta_N \simeq 0.64$, and its Fourier transform

yields $|\mathcal{T}(\omega)| \simeq 0.81$ and $|\mathcal{T}(2\omega)| \simeq 0.50$ at the benchmark, a filter factor $\mathcal{T}(2\omega)/\mathcal{T}(\omega)^2 \simeq 0.76$, in agreement with the closed-form value 0.74 of Eq. (37). This is a reduced solve: it is deterministic, the thermal noise enters only through the fluctuation–dissipation normalization rather than mode by mode, and the $\delta\rho_r$ back-reaction is left out. Even so it reproduces the closed-form filter factor rather than departing from it, which is the check that matters, and supports the robustness of the ratio at the benchmark. The full stochastic computation including the radiation back-reaction remains the outstanding calculation; accordingly we quote $\hat{A}_2/\hat{A}_1^2 \simeq 0.13\text{--}0.19$ — now a single curve set by p and Δ_N , no longer a kernel-shape range — as a stable estimate that the full back-reaction would only refine.

C. Growth function at the feature

The amplitude and slope at $Q_{\text{pk}} \simeq 95$ are set by the scalar dissipation function $G(Q)$. For cubic dissipation we use the WarmSPy-validated form, with the Benetti–Ramos fit as a cross-check [15, 48, 103],

$$\begin{aligned} G(Q) &= 1 + 3.703 Q^{2.613} + 0.0011 Q^{5.721} \quad (p \simeq 5.7), \\ G(Q) &= 1 + 4.981 Q^{1.946} + 0.127 Q^{4.330} \quad (p \simeq 4.3), \end{aligned} \quad (40)$$

both validated over $Q \in [10^{-7}, 10^4]$, so evaluating at the feature is interpolation, not extrapolation. The two differ by a factor $\simeq 7$ in $G(95)$, but this is an *amplitude* difference absorbed by the saturation tuning: it propagates into the required Q_{pk} , $Q_{\text{pk}} \in [74, 123]$, not into the mass scale or the correlated signals. The local slope $p = d \ln G / d \ln Q \simeq 4.3\text{--}5.7$ sets the shape observables. Through $A_2/A_1^2 = (p-1)/(4p)$ it gives an adiabatic ratio $\simeq 0.19\text{--}0.21$ (against 0.150 at $p = 5/2$), bounded in (0.15, 0.25) with asymptote 1/4; the filtered observable is $\hat{A}_2/\hat{A}_1^2 \simeq 0.13\text{--}0.19$, the spread combining the exponent range with the variance-window convention. Both fits agree on these shape observables at the feature, the finite-amplitude saturation washing out their slope difference.

V. PRIMORDIAL BLACK HOLES

When a mode in the enhanced band re-enters the horizon during radiation domination, a rare high-density region can overcome pressure support and collapse to a black hole. We compute the mass fraction with the Press–Schechter prescription [60–62], smoothing the curvature spectrum with a Gaussian window to obtain the variance

$$\sigma^2(M) = \int d \ln k \frac{16}{81} (kR_M)^4 e^{-(kR_M)^2} \mathcal{P}_\zeta(k), \quad (41)$$

where R_M is the comoving horizon scale at formation. The fraction of horizon patches that collapse is

$$\beta(M) = \text{erfc} \left[\frac{\delta_c}{\sqrt{2} \sigma(M)} \right], \quad (42)$$

and the present abundance, normalized to the dark matter, follows by the standard redshift factor [63],

$$f_{\text{PBH}}(M) = \frac{\beta(M)}{1.84 \times 10^{-8}} \left(\frac{M}{M_\odot} \right)^{-1/2}. \quad (43)$$

We take a collapse threshold $\delta_c = 0.414$, representative of the radiation-era value [64–67], and quantify the sensitivity to this choice below. We note that pairing a fixed δ_c with a Gaussian window is not internally consistent at the level of the compaction-function/threshold prescription [68]; since we renormalize the amplitude to saturation, this prescription dependence acts on the (already hand-fixed) amplitude rather than on the mass scale, as quantified below.

The comoving scale k_{pk} fixes the black-hole mass through the horizon mass at re-entry, $M(k_{\text{pk}}) \simeq 30 M_\odot (k_{\text{pk}}/2.9 \times 10^5 \text{ Mpc}^{-1})^{-2} (g_*/10.75)^{-1/6} \simeq 1.4 \times 10^{-12} M_\odot$, using the standard radiation-era calibration [63, 69]. This places the holes in the asteroid-mass window, $M \sim 10^{-16}\text{--}10^{-11} M_\odot$, the one range in which PBHs can still be the entire dark matter: it lies above the evaporation constraints and below the Subaru-HSC and OGLE microlensing bounds [70–72], and our $M \simeq 10^{-12} M_\odot$ peak falls squarely inside it. For the benchmark spectrum, fixing the peak amplitude to $A_{\text{pk}} = 1.12 \times 10^{-2}$ (equivalently $\mathcal{P}_\zeta(k_{\text{pk}}) = 1.7 \times 10^{-2}$) brings the mass function exactly to the saturation line: $\max_M f_{\text{PBH}} = 1.00$, reached at $M \simeq 2.3 \times 10^{-12} M_\odot$, where $\sigma \simeq 0.052$ and $\delta_c/\sigma \simeq 8.0$. Integrating over the mass function,

$$F_{\text{DM}} \equiv \int f_{\text{PBH}}(M) d \ln M \simeq 0.56, \quad (44)$$

so that the integrated fraction is a little over half—the formation-epoch value, before late-time accretion, clustering, or low-mass-edge evaporation shift it. The mass function is narrow, not broad. Because the deep enhancement is a single resonant crossing rather than a comb of equal dips (Sec. II), $f_{\text{PBH}}(M)$ has one peak near $10^{-12} M_\odot$ of width $\sigma_k \simeq 0.5$, with the periodic modulation adding only $\mathcal{O}(\delta)$ ripples on its flanks rather than separate sub-peaks (Fig. 5); the comb valleys never seed a second population. It is therefore not the broad distribution that microlensing and stellar-heating bounds most tightly constrain—those tighten precisely for extended mass functions—and the asteroid window stays open because the abundance is concentrated within it. This number is not a prediction: A_{pk} was *chosen* so that $\max_M f_{\text{PBH}} = 1$, and because β is exponential in the amplitude, a few percent less gives orders of magnitude fewer holes while a few percent more is excluded. Quantitatively, f_{PBH} sweeps the full observable range [$10^{-3}, 1$]

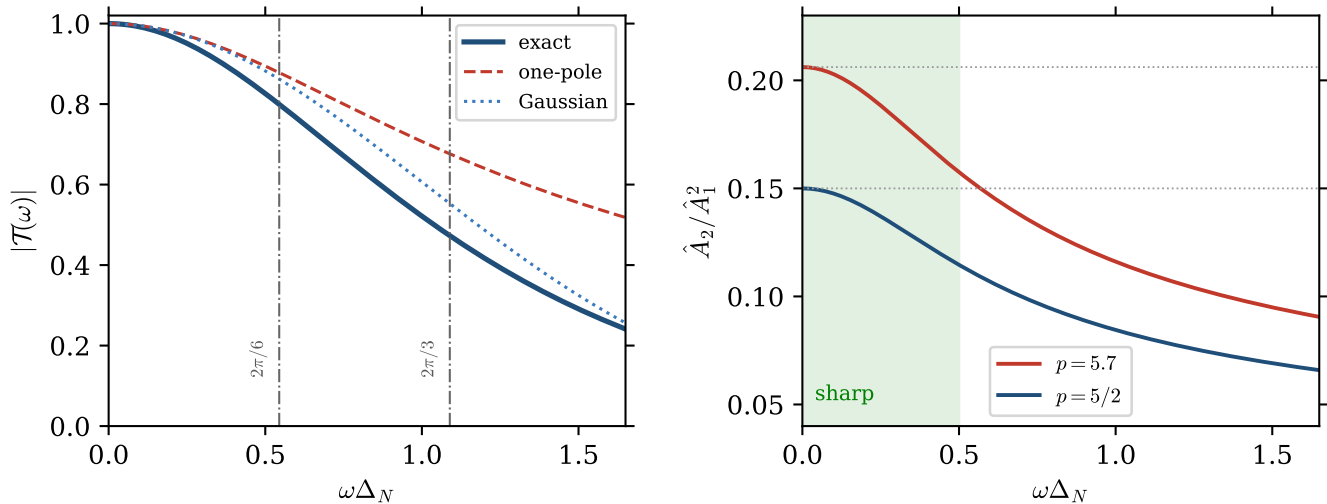


FIG. 4. Left: the freeze-out transfer function $|\mathcal{T}(\omega)|$ of Eq. (37) (solid), derived in closed form from the overdamped Green’s function; the one-pole (red dashed) and Gaussian (blue dotted) kernels of earlier treatments are shown faint and merely bracket it. The benchmark $\omega = 2\pi/6$ and the faster $\omega = 2\pi/3$ are marked (dash-dotted). Right: the filtered harmonic ratio $\hat{A}_2/\hat{A}_1^2 = \frac{3}{20} \mathcal{T}(2\omega)/\mathcal{T}(\omega)^2$ of Eq. (39). The shaded band marks the sharp region $\omega\Delta_N < 0.5$; the dotted line is the adiabatic value for the illustrative exponent $p = 5/2$, recovered as $\omega \rightarrow 0$. For the realistic cubic slope $p \simeq 4.3\text{--}5.7$ both curves scale up by the factor $(p - 1)/(4p) \div (3/20) \simeq 1.3$.

as Q_{pk} moves across the narrow window from 91 to 94—a $\sim 3\%$ interval, equivalently the catalyst dip depth m_0/M_∞ fixed to $\sim 1\%$. This is the exponential sensitivity of the abundance to the spectral amplitude that every PBH-from-inflation scenario shares, not a tuning peculiar to periodic warm inflation. It quantifies the usual PBH abundance tuning: a percent-level adjustment of one catalyst parameter is required for an order-unity PBH fraction, while the correlated GW and phase signatures are far less sensitive to this normalization. What the model predicts robustly is the *mass scale* $M \sim 10^{-12} M_\odot$, set by k_{pk} , together with the correlated gravitational-wave and bispectrum signals of Secs. VI–VII that share the feature’s origin. Figure 5 shows the saturated abundance against the negligible smooth-spectrum result. We now separate which parts of the calculation are stable from which are tuned.

The number that critics of PBH-from-inflation scenarios rightly worry about is β , which depends exponentially on the ratio δ_c/σ . Differentiating, $\partial \ln \beta / \partial \ln \sigma \simeq (\delta_c/\sigma)^2 + 1 \simeq 65$ at our peak ($\delta_c/\sigma \simeq 8$); a one-percent change in σ moves β by a factor of about two. This steepness is not a defect of our model. It is a generic feature of gravitational collapse from a near-Gaussian field with a high threshold, and it afflicts every PBH-dark-matter scenario equally [68, 69, 72–75]. It means that the *overall amplitude* A_{pk} must be specified to percent accuracy to fix f_{PBH} , which is a statement about how finely the inflationary sector is tuned, not about the shape of the prediction.

The shape and the mass scale, by contrast, are stable, and it is worth separating the systematics that act

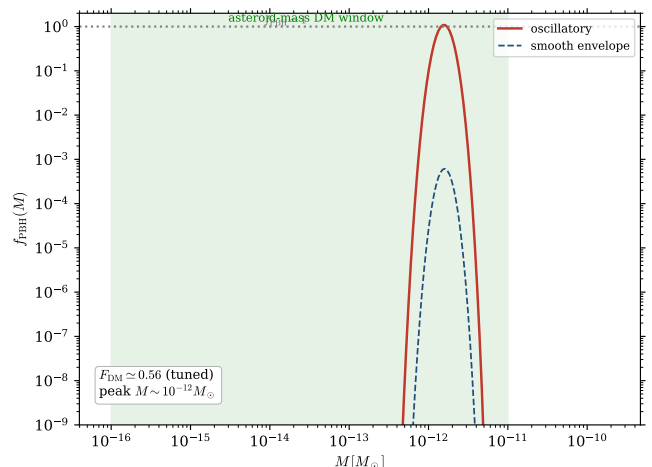


FIG. 5. Differential PBH abundance for the oscillatory (red) and smooth (blue, dashed) spectra. With the peak amplitude tuned so that the mass function just touches the saturation line, $\max_M f_{\text{PBH}} = 1$, the integrated abundance is $F_{\text{DM}} \simeq 0.56$. The smooth spectrum of the same envelope amplitude is utterly negligible, a consequence of the exponential sensitivity discussed in the text.

on the tunable amplitude from those that act on the robust shape. We find that the threshold uncertainty, usually the dominant one, falls in the first class: when the amplitude is renormalized at each step so the mass function continues to touch $f_{\text{PBH}} = 1$, the integrated fraction is essentially independent of the collapse threshold, $F_{\text{DM}} \simeq 0.56$ unchanged as δ_c varies across 0.40–0.50,

TABLE III. Uncertainty budget for the PBH calculation. “Amplitude” systematics are absorbed by the saturation tuning $\max_M f_{\text{PBH}} = 1$; “shape” systematics affect the predicted mass function and scale.

Source	Acts on	Size
Collapse threshold δ_c	amplitude	cancels in shape
Window function	amplitude	$\mathcal{O}(1)$ in A_{pk}
Press–Schechter vs peaks	amplitude	$\mathcal{O}(1\text{--}10)$ in β
Critical collapse (γ)	shape	tens of % in F_{DM}
Non-Gaussianity (equil.)	amplitude	factor few in β
Spectral amplitude A_{pk}	amplitude	exponential; tuned
Freeze-out filtering	modulation	not the abundance

the spread between window-function and compaction-function prescriptions [64, 65]. The threshold acts on the peak amplitude, which we have already fixed by hand, and cancels in the shape.

Three refinements beyond Press–Schechter act on the amplitude, not the mass scale. Critical collapse, $M = \mathcal{K}M_H(\delta - \delta_c)^\gamma$ with $\gamma \simeq 0.357$ [65, 66, 76], broadens the mass function and lowers the peak mass by $\mathcal{O}(1)$, shifting F_{DM} by tens of percent at fixed saturation. Peaks theory rather than Press–Schechter [68, 77] changes β by an $\mathcal{O}(1)$ –10 factor, absorbed by the tuning since β is exponential in δ_c/σ . The equilateral warm bispectrum ($|f_{\text{NL}}| \lesssim 1$) couples weakly to the near-spherical collapse threshold [78], a factor-few amplitude shift. None reaches $F_{\text{DM}} = 1$ from a peaked spectrum: broadening the envelope raises it only slowly, $F_{\text{DM}} = 0.43, 0.56, 0.68, 0.84$ for

$\sigma_k = 0.3, 0.5, 0.7, 1.0$.

It is useful to collect the budget. Table III lists each systematic and whether it acts on the amplitude, which we tune, or on the shape and mass scale, which we predict. The last line is the one connection to Sec. IV B: the $\mathcal{O}(1)$ filtering of the periodic feature suppresses the *oscillation contrast*, not the smooth envelope that sets $\sigma(M)$, so it leaves the abundance untouched and shows up only in the gravitational-wave and bispectrum modulations. The robust outputs of this section are therefore the mass scale $M \sim 10^{-12} M_\odot$ and the existence of the correlated signals; the dark-matter fraction is a tuned normalization carrying an order-of-magnitude systematic spread, and we do not claim it as a prediction.

VI. SCALAR-INDUCED GRAVITATIONAL WAVES

The same enhanced curvature power that forms the black holes also sources tensor modes at second order in perturbation theory [79–81]. This induced background has become a standard probe of small-scale power and of the PBH hypothesis [82, 83]. For a source active during radiation domination the present-day spectral density is

$$h^2\Omega_{\text{GW}}(k) = 1.62 \times 10^{-5} \left(\frac{g_*}{106.75}\right)^{-1/3} \mathcal{I}(k), \quad (45)$$

with the normalization and the redshift factors as in the review of Ref. [84]. The dimensionless integral is

$$\mathcal{I}(k) = \int_0^\infty dv \int_{|1-v|}^{1+v} du \left[\frac{4v^2 - (1+v^2-u^2)^2}{4uv} \right]^2 \overline{I^2(u,v)} \mathcal{P}_\zeta(uk) \mathcal{P}_\zeta(vk), \quad (46)$$

where the time-averaged transfer function in the radiation era is [85, 86]

$$\overline{I^2(u,v)} = \frac{1}{2} \left[\frac{3(u^2 + v^2 - 3)}{4u^3v^3} \right]^2 \left\{ \left[-4uv + (u^2 + v^2 - 3) \ln \left| \frac{3 - (u+v)^2}{3 - (u-v)^2} \right| \right]^2 + \pi^2(u^2 + v^2 - 3)^2 \Theta(u+v-\sqrt{3}) \right\}. \quad (47)$$

We evaluate Eq. (46) by changing to the variables $t = u + v - 1$ and $s = u - v$, which map the kinematic triangle onto the rectangle $t \in [0, \infty)$, $s \in [-1, 1]$ and isolate the logarithmic resonance at $t = \sqrt{3} - 1$ as a single interior breakpoint. As a numerical accuracy check we vary the relative quadrature tolerance over $\epsilon_{\text{rel}} \in [10^{-4}, 10^{-7}]$ and the upper cutoff over $t_{\text{max}} \in [8, 20]$; the peak value $h^2\Omega_{\text{GW}}^{\text{pk}} = 1.36 \times 10^{-8}$ is stable to better than one percent, confirming that the resonance and the slowly converging tail are both captured. This is the full kernel, not an envelope approximation; dropping the polarization prefactor or the u^3v^3 structure of Eq. (47) distorts both the peak and the infrared slope.

The result, obtained by integrating the kernel Eq. (47) directly over the full curvature spectrum with no analytic approximation to the convolution, is shown in Fig. 6; our prefactor and kernel conventions, including the factors of π in the resonant $u + v = \sqrt{3}$ term, follow Refs. [85, 86] exactly, so the normalization carries no residual factor-of-two ambiguity. The spectrum peaks at

$$h^2\Omega_{\text{GW}}^{\text{pk}} \simeq 1.4 \times 10^{-8} \quad \text{at} \quad f_{\text{pk}} \simeq 3.1 \text{ mHz}, \quad (48)$$

where the conversion $f = 1.55 \times 10^{-15} (k/\text{Mpc}^{-1}) \text{ Hz}$ puts it squarely in the LISA band [87, 88]. This is about five orders of magnitude above the nominal LISA sensitivity [89], and its height is not a free dial: the satu-

ration condition $\max_M f_{\text{PBH}} = 1$ fixes the peak curvature power, hence $h^2\Omega_{\text{GW}} \sim 10^{-8}$, almost independently of δ and ω . The one lever that moves it is the PBH fraction—were the holes subdominant, the peak would fall in proportion—so “within LISA’s reach” rests on the PBHs being a substantial part of the dark matter, not on the optimistic end of the dissipation parameters. A genuine signal-to-noise would need the LISA response and noise folded in, which we have not done. Below the peak the spectrum rises with the causal slope $n_{\text{GW}} \rightarrow 3$ in the deep infrared, modified by the standard logarithmic running [90, 91]; the spurious infrared rise of a truncated kernel is absent. The post-peak dip of the curvature spectrum (Fig. 3) is largely washed out by the convolution, surviving only as a $\lesssim 10\%$ suppression on the ultraviolet flank of the peak—present in both bands but too shallow to resolve on its own. Two effects low-pass the comb on its way into the GW background: the broad convolution of the induced-GW kernel, and the acoustic oscillations of the plasma at horizon re-entry, which smear curvature features narrower than the sound horizon. The GW comb is therefore shallower than the primordial one—visible in the residual modulation of Fig. 6 but smeared relative to Fig. 3. Whether it is *resolvable*, as opposed to merely present, is a question of instrument response we do not settle here: the LISA peak sits at $h^2\Omega_{\text{GW}} \sim 10^{-8}$, well above the projected sensitivity, so the $\mathcal{O}(\delta)$ modulation is in principle measurable, but a quantitative signal-to-noise forecast folding in the LISA response and noise is left to future work.

The spectrum does not end at the peak. As the inflaton rolls on Q keeps growing, so the curvature power climbs back toward $\mathcal{P}_\zeta \sim 5 \times 10^{-4}$ over many decades, sourcing a *second* induced-GW band: $k \sim 10^{14}\text{--}10^{17}$ Mpc $^{-1}$ maps to $f \sim 0.1\text{--}10^2$ Hz at $h^2\Omega_{\text{GW}} \sim 10^{-11}$, within DECIGO [92] and Einstein Telescope [93, 94] reach, far above the PTA band [95]. It carries the same ω and ψ as the LISA peak—one log-periodic signal seen 10^4 apart, not two backgrounds. Overproduction caps it ($\mathcal{P}_\zeta \lesssim 10^{-2}$ throughout), and $\int h^2\Omega_{\text{GW}} d\ln f$ gives $\Delta N_{\text{eff}} \sim 10^{-3}$, inside the BBN bound [83]. The tail amplitude is a benchmark (the post-feature Q -profile depends on how inflation ends); robust is that a second, phase-locked band is generic.

Because the induced spectrum is a convolution of two copies of \mathcal{P}_ζ , the log-periodic feature is not transmitted unchanged. The quadratic source mixes the fundamental with its second harmonic and partially averages both over the convolution window, so the residual carries power at ω and 2ω with comparable weight.

The structure follows semi-analytically. Write $\mathcal{P}_\zeta(uk) = \mathcal{A}(uk)[1+m(uk)]$ with $m(uk) = A_1 \cos \omega(\ln k + \ln u) + A_2 \cos 2\omega(\ln k + \ln u)$. The fractional residual is then

$$\begin{aligned} r(\ln k) &= \frac{\Omega_{\text{GW}}^{\text{osc}}}{\Omega_{\text{GW}}^{\text{sm}}} - 1 \\ &= \langle m(uk) + m(vk) + m(uk)m(vk) \rangle_w, \end{aligned} \quad (49)$$

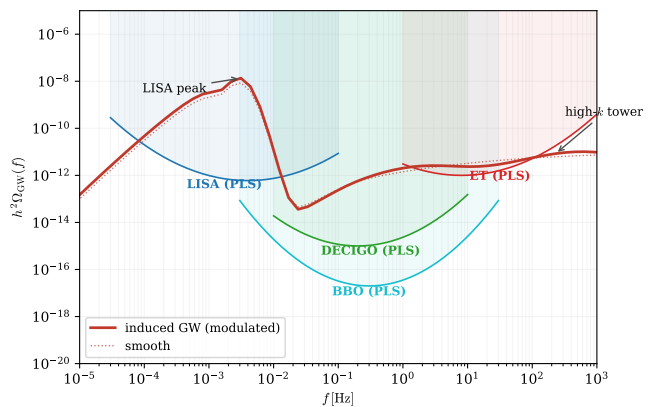


FIG. 6. Power-law-integrated sensitivity (PLS) curves (SNR = 10) for LISA, DECIGO, BBO, and ET follow Ref. [96]. Induced gravitational-wave background from the full curvature spectrum, computed with the radiation-era kernel of Eqs. (46)–(47) for the benchmark $\delta = 0.2$, $\omega = 2\pi/6$, against those of LISA, DECIGO, BBO, and the Einstein Telescope (ET). The resonant peak gives the LISA signal near 3 mHz, $h^2\Omega_{\text{GW}} \simeq 1.4 \times 10^{-8}$; the continued growth of the dissipation toward smaller scales feeds a second band at $h^2\Omega_{\text{GW}} \sim 10^{-11}$ from deci-hertz to a hundred hertz, within DECIGO/ET reach. Both bands carry the same log-period ω and freeze-out phase ψ . The dotted curve is the unmodulated envelope; the quadratic source low-passes the comb, so the multi-decade oscillation of \mathcal{P}_ζ survives only as the broad two-band envelope.

where $\langle \cdot \rangle_w$ is the average over the (u, v) plane weighted by $w = [\dots]^2 \bar{I}^2 \mathcal{A}(uk)\mathcal{A}(vk)$. Defining the kernel form factors $C_n = \langle \cos(n\omega \ln u) \rangle_w$, the linear terms contribute $2A_1C_1 \cos(\omega \ln k) + 2A_2C_2 \cos(2\omega \ln k)$, while the product term contributes a sum-frequency piece $\frac{1}{2}A_1^2C' \cos(2\omega \ln k)$ that the convolution generates from the square of the fundamental. Hence

$$B_1 \simeq 2A_1C_1, \quad B_2 \simeq 2A_2C_2 + \frac{1}{2}A_1^2C', \quad (50)$$

which already explains the two qualitative facts: B_1 is of order A_1 times a form factor, and B_2 is not small because it inherits a piece $\propto A_1^2$ from the self-convolution of the fundamental rather than only the genuine second harmonic A_2 . Evaluating the form factors at the peak gives $C_1 = 0.96$, $C_2 = 0.74$, $C' = 0.92$, so $2A_1C_1 = 0.96$ sets the scale of the fundamental and the product term keeps B_2 a non-negligible fraction of B_1 . The peak-local estimate overshoots the band value because, away from the peak, the weight shifts to $\ln u \neq 0$ and the resulting $\langle \sin \rangle \neq 0$ partially cancels the cosine projection; the semi-analytic argument fixes the scale and the multi-harmonic structure, while the precise band-averaged amplitudes come from the fit below.

Fitting $r(\ln k)$ to a slow baseline plus harmonics at $\omega, 2\omega$, the slow benchmark costs us: spanning less than one cycle in band, the amplitude is not sharply pinned, $B_1 \simeq 0.5\text{--}1.3$ (a third from the $\mathcal{O}(10\%)$ drift of Sec. III, the rest baseline ambiguity). We quote $B_1 = \mathcal{O}(1)$ with

B_2 a sizable fraction, consistent with $2A_1C_1 \simeq 0.96$. This is the converse of Sec. IV B: the GW oscillation is cleanest at fast modulation where the ratio blurs, and sharp at slow modulation where it goes marginal—the limit is geometry, fewer than one log-period in band.

VII. THE BISPECTRUM AND ITS PHASE

The third signal lives in the three-point function. Warm inflation produces a non-Gaussianity of the equilateral type, with a sign and magnitude controlled by the dissipation [97, 98]. In the strong regime the smooth, non-oscillatory part is

$$f_{\text{NL}}^{\text{bg}} = -\frac{5}{12} \frac{1+7Q_0/4}{1+Q_0} \simeq -0.72 \quad (51)$$

for $Q_0 = 50$, consistent in sign and strong-dissipation magnitude with the warm-inflation bispectrum results cited above. The periodic modulation adds an oscillatory piece whose amplitude is

$$f_0 = -\frac{5}{12} \frac{\omega Q_0 \delta}{1+Q_0} \simeq -0.086, \quad (52)$$

so that the total stays small, $|f_{\text{NL}}| \lesssim 0.9$, comfortably within the Planck equilateral bound $f_{\text{NL}}^{\text{equil}} = -26 \pm 47$ [99]. The feature is therefore not constrained by current CMB non-Gaussianity, and its interest is structural rather than amplitude-based.

The structure follows from how the warm bispectrum is generated. In warm inflation the equilateral non-Gaussianity is not a primordial vertex but is induced as the modes cross the horizon, and for a feature it is dominated by the variation of the background dissipative quantities across that feature. To the accuracy we work at, the oscillatory part of the equilateral f_{NL} tracks the logarithmic running of the curvature spectrum,

$$\delta f_{\text{NL}}(k) \simeq c_a \frac{d \delta \ln \mathcal{P}_\zeta}{d \ln k}, \quad (53)$$

with c_a a slowly varying coefficient of order $\omega Q_0 \delta / (1 + Q_0)$ fixed by the warm vertex of Refs. [97, 98]. Equation (53) follows from a separate-universe argument, the warm counterpart of the background-wave derivation of the single-field consistency relation [35, 100]. A long-wavelength mode ζ_L shifts the local number of e-folds and, at freeze-out, the argument of the small-scale feature,

$$\mathcal{P}_\zeta(k)|_{\zeta_L} = \mathcal{P}_\zeta(k e^{-\zeta_L}) \simeq \mathcal{P}_\zeta(k) \left[1 - \zeta_L \frac{d \ln \mathcal{P}_\zeta}{d \ln k} \right], \quad (54)$$

so the squeezed three-point function is $\langle \zeta_L \zeta_k \zeta_k \rangle' = -(d \ln \mathcal{P}_\zeta / d \ln k) P_L \mathcal{P}_\zeta(k)$: the non-Gaussianity tracks the running. The equilateral configuration relevant to the warm bispectrum inherits the same structure, since for a feature sharp in $\ln k$ the bispectrum is dominated by

the variation of the background across the feature rather than by the smooth shape function. Two steps remain imported rather than derived in the warm setting — the coefficient c_a from the cubic dissipative vertex, and the squeezed-to-equilateral inheritance, which we take on the cold-feature logic [29, 33] — so we present the $\pi/2$ offset as a leading-order expectation rather than a firm prediction, the least-established of the three. The point is then purely kinematic. If the filtered power-spectrum modulation is $\delta \ln \mathcal{P}_\zeta = \hat{A}_1 \cos(\omega \ln k + \psi)$, where $\psi = \arg \mathcal{T}(\omega)$ is the phase picked up from the freeze-out filter of Sec. IV B, then

$$\delta f_{\text{NL}} \simeq -c_a \omega \hat{A}_1 \sin(\omega \ln k + \psi), \quad (55)$$

which is exactly a quarter cycle ahead of $\delta \ln \mathcal{P}_\zeta$. The filter phase ψ appears identically in both, so it cancels in the relative phase: the $\pi/2$ offset is independent of the kernel shape that we could not pin down for the amplitudes. This is an approximate but genuine analytical result, not a conjecture: the quarter-cycle offset follows structurally from f_{NL} tracking the running of \mathcal{P}_ζ , since $d/d \ln k [\cos(\omega \ln k)] = -\omega \sin(\omega \ln k)$; the warm three-point vertex we have not computed can renormalize the coefficient c_a but cannot move the $\pi/2$, which is fixed by that derivative relation. As shown in Fig. 7, the two features are in quadrature. This is what distinguishes the present scenario from the resonant non-Gaussianity of cold axion-monodromy inflation, where the bispectrum oscillation is generated by the same potential feature that drives the power-spectrum oscillation and the two are in phase [25, 28, 101]. A measured quarter-cycle offset would be hard to fake with a cold-inflation feature and would point specifically at a dissipative origin.

A calculable correction enters where the $\pi/2$ is not protected: beyond the running term of Eq. (53), the modulation also feeds the cubic vertex directly, filtered by its own \mathcal{T}_3 , shifting the offset by

$$\Delta - \frac{\pi}{2} \simeq \frac{c_b}{c_a \omega \hat{A}_1} |\mathcal{T}_3| \cos(\psi_3 - \psi), \quad (56)$$

with $\psi_3 = \arg \mathcal{T}_3$. Since $c_a \sim \omega Q_0 \delta / (1 + Q_0)$ is enhanced in the strong regime while c_b is slow-roll suppressed, $|\Delta - \pi/2| \lesssim 0.1\text{--}0.2$ rad: the phase drifts only sub-leadingly, unlike the $\mathcal{O}(1)$ amplitude suppression of Sec. IV B. Two gaps keep it an expectation: pinning c_b needs the full modulated cubic vertex, and the squeezed separate-universe argument's inheritance by the equilateral configuration follows cold-feature logic [29] not yet shown for the warm vertex. It is the conjectural member of the triple.

VIII. OBSERVATIONAL PROSPECTS AND FALSIFIABILITY

A model of this kind earns its keep by how it can be killed. The scenario ties several observables to one periodic modulation, and the links between them are sharper than any single amplitude.

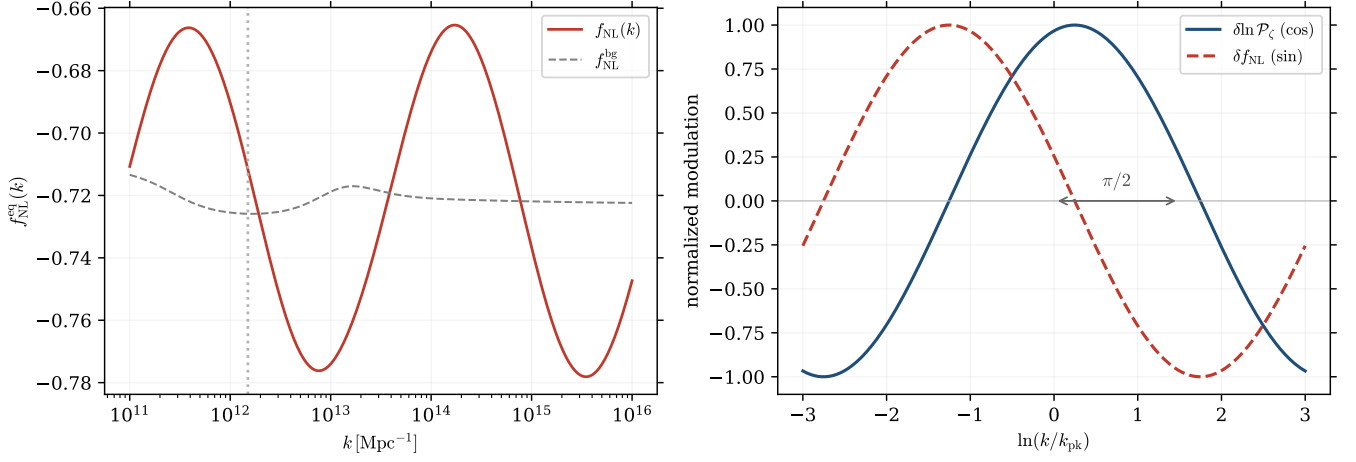


FIG. 7. Left: the equilateral non-Gaussianity $f_{\text{NL}}^{\text{eq}}(k)$ across the feature (red), oscillating about the smooth warm value $f_{\text{NL}}^{\text{bg}} \simeq -0.73$ (dashed). Right: the phase relation between the power-spectrum modulation ($\propto \cos \omega \ln k$, blue) and the oscillatory part of f_{NL} ($\propto \sin \omega \ln k$, red dashed); the quarter-cycle offset $\Delta = \pi/2$ follows from f_{NL} tracking the running of \mathcal{P}_ζ , and is the signature absent in cold-inflation feature models.

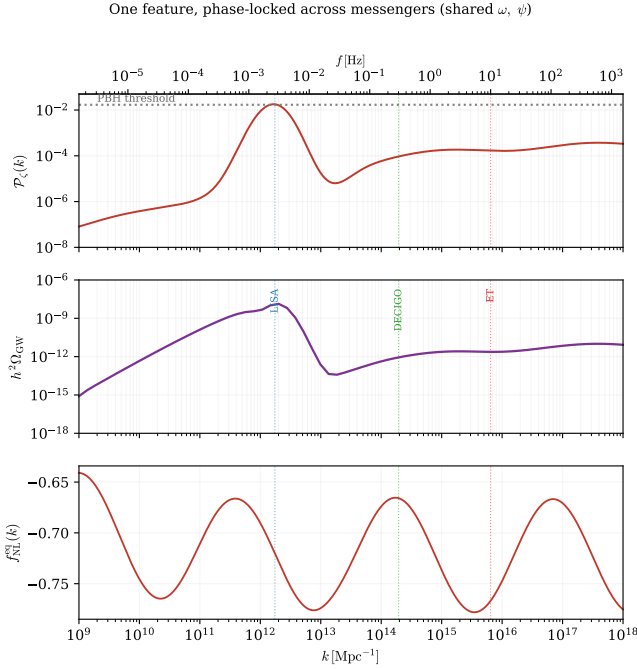


FIG. 8. The correlated signature: the three observables on a common wavenumber axis, with detector centre frequencies marked. Top: the curvature spectrum, with its resonant peak at the PBH threshold and the rising small-scale tail. Middle: the induced GW background, peaking in the LISA band and rising again into the DECIGO/ET band. Bottom: the equilateral f_{NL} . All three carry the log-period ω and freeze-out phase ψ of the underlying friction, so a signal in one channel fixes where to look in the others.

The sharpest is the multiband GW locking. The LISA peak and the high-frequency tower (Sec. VI) come from

one feature at scales 10^4 apart, sharing ω and ψ . In Fig. 8 the GW peak falls at the image of the curvature peak under $f = 1.55 \times 10^{-15} (k/\text{Mpc}^{-1})$ Hz and the tower at the image of the rising tail, read off the same computation; a background in both the millihertz and deci-to-hectohertz bands modulated at one ω is not what a foreground or a single-scale feature produces. The remaining links tie the power spectrum to the rest: the harmonic ratio $A_2/A_1^2 = (p-1)/(4p)$ is fixed by the slope $p \simeq 4.3\text{--}5.7$ (observable 0.13–0.19 after filtering, $\leq 1/4$); the same δ sets the GW depths B_1, B_2 via Eq. (50); and the bispectrum runs a quarter cycle ahead, a robust result for cold features [25, 102] imported here in the separate-universe limit and protected by the common filter—the least firmly derived of the three but, if the warm three-point computation confirm it, the most filter protected.

Several things still have to fall into place. Reaching the PBH amplitude drives the dissipation to $Q_{\text{pk}} \simeq 95$; this is interpolation, not extrapolation, since the WarmSPy fits are validated over $Q \in [10^{-7}, 10^4]$ [48], and a factor-of-three error in $\mathcal{P}_\zeta \propto G(Q) \sim Q^{4.3}$ moves the required Q_{pk} only to $\simeq 74\text{--}123$ (Sec. IV C). The blue CMB tilt is fixed by placing the pivot in the weak-dissipation regime with an effective $F \simeq 5$, giving $n_s \simeq 0.965$ and, for the plateau completion, $r \simeq 4 \times 10^{-3}$ —viable, but no longer minimal. The PBH abundance is tuned to saturation, so the robust output is the mass scale, not the dark-matter fraction (Table III). And the freeze-out kernel that controls the $\mathcal{O}(1)$ filtering of the feature awaits the full stochastic solve. These qualify the amplitudes; the correlated, multiband structure is what we would stake the scenario on.

IX. CONCLUSIONS

The premise is narrow—an axion-like inflaton whose dissipation is periodic in the field, deep in the strong regime—and the paper traces where it leads. The background and curvature spectrum follow directly from the warm equations; the bispectrum phase and PBH abundance carry the systematics of the three-point vertex and stochastic back-reaction. The modulation writes a log-periodic feature on the small-scale spectrum and leaves the CMB untouched, the pivot at $Q \ll 1$. Its response to the time-dependent friction is governed by a closed-form freeze-out transfer function controlled by $\omega\Delta_N$, not the ω/\sqrt{Q} of naive counting; at the slow benchmark the filtering is mild and the harmonic ratio stays sharp, bounded by $1/4$.

Tuned to saturation, the feature makes primordial black holes near $10^{-12} M_\odot$ —a robust mass scale, a tuned fraction. It sources gravitational waves in two bands: a LISA peak at $h^2\Omega_{\text{GW}} \sim 10^{-8}$ near 3 mHz, and a higher-frequency tower at $\sim 10^{-11}$ reaching DECIGO and the Einstein Telescope, fed by the continued growth of the friction and capped by black-hole overproduction. And separate-universe arguments suggest it shifts the equilateral bispectrum a quarter cycle from the power

spectrum—a theorem for cold resonant features [25], here a motivated hypothesis awaiting the warm three-point computation. All of these carry one ω and one ψ , so they stand or fall together; that correlation—across two decades of frequency and three observables—is what makes the scenario testable rather than merely viable.

Provisional elements remain: a tuned abundance, a growth function pushed to the feature amplitude, a CMB sector that needs a plateau completion. They qualify the amplitudes, not the correlated structure. The open theoretical task is a full mode-by-mode treatment of the modulated friction, which would fix the freeze-out kernel and carry the sharp predictions of the slow regime to any modulation frequency. The high-frequency GW tower, bounded by overproduction, is the most immediately actionable piece, and turning that bound quantitative is the natural next step.

ACKNOWLEDGMENTS

The work of M.R.G. is supported by the Science and Engineering Research Board (SERB), DST, Government of India, under Grant No. CRG/2022/004120 (Core Research Grant). M.R.G. thanks IUCAA, Pune, for hospitality during an associate visit where this work was initiated.

-
- [1] A. Berera and L. Z. Fang, Phys. Rev. Lett. **74**, 1912 (1995).
 - [2] A. Berera, Phys. Rev. Lett. **75**, 3218 (1995).
 - [3] A. Berera, M. Gleiser, and R. O. Ramos, Phys. Rev. D **58**, 123508 (1998), arXiv:hep-ph/9803394.
 - [4] A. Berera, I. G. Moss, and R. O. Ramos, Rept. Prog. Phys. **72**, 026901 (2009), arXiv:0808.1855.
 - [5] M. Bastero-Gil and A. Berera, Int. J. Mod. Phys. A **24**, 2207 (2009), arXiv:0902.0521.
 - [6] A. Berera, Phys. Rev. D **55**, 3346 (1997), arXiv:hep-ph/9612239.
 - [7] J. Yokoyama and A. D. Linde, Phys. Rev. D **60**, 083509 (1999), arXiv:hep-ph/9809409.
 - [8] M. Bastero-Gil, A. Berera, and R. O. Ramos, JCAP **09**, 033 (2011), arXiv:1008.1929.
 - [9] A. Berera and R. O. Ramos, Phys. Rev. D **71**, 023513 (2005), arXiv:hep-ph/0406339.
 - [10] A. Berera and T. W. Kephart, Phys. Rev. Lett. **83**, 1084 (1999), arXiv:hep-ph/9904410.
 - [11] M. Laine and S. Proccacci, JCAP **06**, 031 (2021), arXiv:2102.09913.
 - [12] M. Bastero-Gil, A. Berera, R. O. Ramos, and J. G. Rosa, Phys. Rev. Lett. **117**, 151301 (2016), arXiv:1604.08838.
 - [13] M. Bastero-Gil, A. Berera, R. O. Ramos, and J. G. Rosa, JCAP **01**, 016 (2013), arXiv:1207.0445.
 - [14] M. Bastero-Gil, A. Berera, R. O. Ramos, and J. G. Rosa, Phys. Lett. B **813**, 136055 (2021), arXiv:1907.13410.
 - [15] M. Benetti and R. O. Ramos, Phys. Rev. D **95**, 023517 (2017), arXiv:1610.08758.
 - [16] M. Bastero-Gil, S. Bhattacharya, K. Dutta, and M. R. Gangopadhyay, JCAP **02**, 054 (2018), arXiv:1710.10008.
 - [17] Y. Akrami *et al.* (Planck Collaboration), Astron. Astrophys. **641**, A10 (2020), arXiv:1807.06211.
 - [18] A. Berera, J. Mabillard, M. Pieroni, and R. O. Ramos, JCAP **07**, 021 (2018), arXiv:1803.04982.
 - [19] M. R. Gangopadhyay, S. Myrzakul, M. Sami, and M. K. Sharma, Phys. Rev. D **103**, 043505 (2021), arXiv:2011.09155.
 - [20] S. Basak, S. Bhattacharya, M. R. Gangopadhyay, N. Jaman, R. Rangarajan, and M. Sami, JCAP **03**, 063 (2022), arXiv:2110.00607.
 - [21] K. Freese, J. A. Frieman, and A. V. Olinto, Phys. Rev. Lett. **65**, 3233 (1990).
 - [22] E. Silverstein and A. Westphal, Phys. Rev. D **78**, 106003 (2008), arXiv:0803.3085.
 - [23] L. McAllister, E. Silverstein, and A. Westphal, Phys. Rev. D **82**, 046003 (2010), arXiv:0808.0706.
 - [24] R. Flauger, L. McAllister, E. Pajer, A. Westphal, and G. Xu, JCAP **06**, 009 (2010), arXiv:0907.2916.
 - [25] R. Flauger and E. Pajer, JCAP **01**, 017 (2011), arXiv:1002.0833.
 - [26] S. Hannestad, T. Haugbolle, P. R. Jarnhus, and M. S. Sloth, JCAP **06**, 001 (2010), arXiv:0912.3527.
 - [27] R. Flauger, L. McAllister, E. Silverstein, and A. Westphal, JCAP **10**, 055 (2017), arXiv:1412.1814.
 - [28] S. R. Behbahani, A. Dymarsky, M. Mirbabayi, and L. Senatore, JCAP **12**, 036 (2012), arXiv:1111.3373.

- [29] X. Chen, R. Easther, and E. A. Lim, *JCAP* **04**, 010 (2008), arXiv:0801.3295.
- [30] X. Chen, *Adv. Astron.* **2010**, 638979 (2010), arXiv:1002.1416.
- [31] T. Kobayashi and F. Takahashi, *JCAP* **01**, 026 (2011), arXiv:1011.3988.
- [32] A. Achúcarro, J.-O. Gong, S. Hardeman, G. A. Palma, and S. P. Patil, *JCAP* **01**, 030 (2011), arXiv:1010.3693.
- [33] X. Chen, *JCAP* **01**, 038 (2012), arXiv:1104.1323.
- [34] E. Pajer and M. Peloso, *Class. Quant. Grav.* **30**, 214002 (2013), arXiv:1305.3557.
- [35] J. M. Maldacena, *JHEP* **05**, 013 (2003), arXiv:astro-ph/0210603.
- [36] V. Acquaviva, N. Bartolo, S. Matarrese, and A. Riotto, *Nucl. Phys. B* **667**, 119 (2003), arXiv:astro-ph/0209156.
- [37] D. Babich, P. Creminelli, and M. Zaldarriaga, *JCAP* **08**, 009 (2004), arXiv:astro-ph/0405356.
- [38] X. Chen, M.-x. Huang, S. Kachru, and G. Shiu, *JCAP* **01**, 002 (2007), arXiv:hep-th/0605045.
- [39] R. Arya, *JCAP* **09**, 042 (2020), arXiv:1910.05238.
- [40] M. Correa, M. R. Gangopadhyay, N. Jaman, and G. J. Mathews, *Phys. Lett. B* **835**, 137510 (2022), arXiv:2207.10394.
- [41] M. Correa, M. R. Gangopadhyay, N. Jaman, and G. J. Mathews, *Phys. Rev. D* **109**, 063539 (2024), arXiv:2306.09641.
- [42] R. Arya, R. K. Jain, and A. K. Mishra, *JCAP* **02**, 034 (2024), arXiv:2302.08940.
- [43] A. Ito and R. O. Ramos, *JCAP* **08**, 076 (2025), arXiv:2504.15606.
- [44] M. Bastero-Gil, A. Berera, R. O. Ramos, and J. G. Rosa, *Phys. Lett. B* **712**, 425 (2012), arXiv:1110.3971.
- [45] J. G. Rosa and L. B. Ventura, *Phys. Rev. Lett.* **122**, 161301 (2019), arXiv:1811.05493.
- [46] K. V. Berghaus, P. W. Graham, and D. E. Kaplan, *JCAP* **03**, 034 (2020) [Erratum: *JCAP* **10**, E02 (2023)], arXiv:1910.07525.
- [47] S. Zell, *Phys. Rev. D* **112**, L081307 (2025), arXiv:2408.07746 [hep-ph].
- [48] G. Montefalcone, V. Aragam, L. Visinelli, and K. Freese, *JCAP* **01**, 032 (2024), arXiv:2306.16190.
- [49] R. O. Ramos and L. A. da Silva, *JCAP* **03**, 032 (2013), arXiv:1302.3544.
- [50] P. A. R. Ade *et al.* (BICEP/Keck Collaboration), *Phys. Rev. Lett.* **127**, 151301 (2021), arXiv:2110.00483.
- [51] J. E. Kim, H. P. Nilles, and M. Peloso, *JCAP* **01**, 005 (2005), arXiv:hep-ph/0409138.
- [52] C. Graham and I. G. Moss, *JCAP* **07**, 013 (2009), arXiv:0905.3500.
- [53] M. Bastero-Gil, A. Berera, I. G. Moss, and R. O. Ramos, *JCAP* **05**, 004 (2014), arXiv:1401.1149.
- [54] L. Visinelli, *JCAP* **01**, 005 (2015), arXiv:1410.1187.
- [55] M. Bastero-Gil, A. Berera, and R. O. Ramos, *JCAP* **07**, 030 (2011), arXiv:1106.0701.
- [56] M. Bastero-Gil, A. Berera, R. Brandenberger, I. G. Moss, R. O. Ramos, and J. G. Rosa, *JCAP* **01**, 002 (2018), arXiv:1612.04726.
- [57] M. R. Gangopadhyay, J. C. Jain, D. Sharma, and Yogesh, *Eur. Phys. J. C* **82**, 849 (2022), arXiv:2108.13839.
- [58] S. Choudhury, M. R. Gangopadhyay, and M. Sami, *Eur. Phys. J. C* **84**, 884 (2024), arXiv:2301.10000.
- [59] M. R. Gangopadhyay and N. Kumar, *Phys. Dark Univ.* **52** (2026), arXiv:2603.11629.
- [60] W. H. Press and P. Schechter, *Astrophys. J.* **187**, 425 (1974).
- [61] B. J. Carr and S. W. Hawking, *Mon. Not. R. Astron. Soc.* **168**, 399 (1974).
- [62] B. J. Carr, *Astrophys. J.* **201**, 1 (1975).
- [63] A. M. Green and B. J. Kavanagh, *J. Phys. G* **48**, 043001 (2021), arXiv:2007.10722.
- [64] I. Musco, *Phys. Rev. D* **100**, 123524 (2019), arXiv:1809.02127.
- [65] T. Harada, C.-M. Yoo, and K. Kohri, *Phys. Rev. D* **88**, 084051 (2013) [Erratum: *Phys. Rev. D* **89**, 029903 (2014)], arXiv:1309.4201.
- [66] J. C. Niemeyer and K. Jedamzik, *Phys. Rev. D* **59**, 124013 (1999), arXiv:astro-ph/9901292.
- [67] M. Shibata and M. Sasaki, *Phys. Rev. D* **60**, 084002 (1999), arXiv:gr-qc/9905064.
- [68] S. Young, C. T. Byrnes, and M. Sasaki, *JCAP* **07**, 045 (2014), arXiv:1405.7023.
- [69] B. Carr, K. Kohri, Y. Sendouda, and J. Yokoyama, *Rept. Prog. Phys.* **84**, 116902 (2021), arXiv:2002.12778.
- [70] H. Niihara *et al.*, *Nat. Astron.* **3**, 524 (2019), arXiv:1701.02151.
- [71] H. Niihara, M. Takada, S. Yokoyama, T. Sumi, and S. Masaki, *Phys. Rev. D* **99**, 083503 (2019), arXiv:1901.07120.
- [72] B. Carr and F. Kühnel, *Ann. Rev. Nucl. Part. Sci.* **70**, 355 (2020), arXiv:2006.02838.
- [73] M. Sasaki, T. Suyama, T. Tanaka, and S. Yokoyama, *Class. Quant. Grav.* **35**, 063001 (2018), arXiv:1801.05235.
- [74] B. Carr, F. Kühnel, and M. Sandstad, *Phys. Rev. D* **94**, 083504 (2016), arXiv:1607.06077.
- [75] B. Carr, F. Kühnel, and L. Visinelli, *Mon. Not. R. Astron. Soc.* **501**, 2029 (2021), arXiv:2008.08077.
- [76] M. W. Choptuik, *Phys. Rev. Lett.* **70**, 9 (1993).
- [77] C.-M. Yoo, T. Harada, J. Garriga, and K. Kohri, *PTEP* **2018**, 123E01 (2018), arXiv:1805.03946.
- [78] V. Atal and C. Germani, *Phys. Dark Univ.* **24**, 100275 (2019), arXiv:1811.07857.
- [79] K. N. Ananda, C. Clarkson, and D. Wands, *Phys. Rev. D* **75**, 123518 (2007), arXiv:gr-qc/0612013.
- [80] D. Baumann, P. J. Steinhardt, K. Takahashi, and K. Ichiki, *Phys. Rev. D* **76**, 084019 (2007), arXiv:hep-th/0703290.
- [81] R. Saito and J. Yokoyama, *Phys. Rev. Lett.* **102**, 161101 (2009); **107**, 069901(E) (2011), arXiv:0812.4339.
- [82] N. Bartolo, V. De Luca, G. Franciolini, M. Peloso, D. Racco, and A. Riotto, *Phys. Rev. D* **99**, 103521 (2019), arXiv:1810.12224.
- [83] C. Caprini and D. G. Figueroa, *Class. Quant. Grav.* **35**, 163001 (2018), arXiv:1801.04268.
- [84] G. Domènech, *Universe* **7**, 398 (2021), arXiv:2109.01398.
- [85] K. Kohri and T. Terada, *Phys. Rev. D* **97**, 123532 (2018), arXiv:1804.08577.
- [86] J. R. Espinosa, D. Racco, and A. Riotto, *JCAP* **09**, 012 (2018), arXiv:1804.07732.
- [87] P. Amaro-Seoane *et al.* (LISA Collaboration), arXiv:1702.00786.
- [88] M. Colpi *et al.* (LISA Collaboration), arXiv:2402.07571.
- [89] T. Robson, N. J. Cornish, and C. Liu, *Class. Quant. Grav.* **36**, 105011 (2019), arXiv:1803.01944.
- [90] C. Yuan, Z.-C. Chen, and Q.-G. Huang, *Phys. Rev. D* **101**, 043019 (2020), arXiv:1910.09099.

- [91] R.-G. Cai, S. Pi, and M. Sasaki, *Phys. Rev. Lett.* **122**, 201101 (2019), arXiv:1810.11000.
- [92] S. Kawamura *et al.*, *Class. Quant. Grav.* **28**, 094011 (2011).
- [93] M. Punturo *et al.*, *Class. Quant. Grav.* **27**, 194002 (2010).
- [94] M. Maggiore *et al.*, *JCAP* **03**, 050 (2020), arXiv:1912.02622.
- [95] G. Agazie *et al.* (NANOGrav Collaboration), *Astrophys. J. Lett.* **951**, L8 (2023), arXiv:2306.16213.
- [96] K. Schmitz, *JHEP* **01**, 097 (2021), arXiv:2002.04615 [hep-ph].
- [97] I. G. Moss and C. Xiong, *JCAP* **04**, 007 (2007), arXiv:astro-ph/0701302.
- [98] I. G. Moss and T. Yeomans, *JCAP* **08**, 009 (2011), arXiv:1102.2833.
- [99] Y. Akrami *et al.* (Planck Collaboration), *Astron. Astrophys.* **641**, A9 (2020), arXiv:1905.05697.
- [100] P. Creminelli and M. Zaldarriaga, *JCAP* **10**, 006 (2004), arXiv:astro-ph/0407059.
- [101] S. R. Behbahani and D. Green, *JCAP* **11**, 056 (2012), arXiv:1207.2779.
- [102] P. Adshead, C. Dvorkin, W. Hu, and E. A. Lim, *Phys. Rev. D* **85**, 023531 (2012), arXiv:1110.3050.
- [103] M. Bastero-Gil, A. Berera, R. O. Ramos, and J. G. Rosa, *JHEP* **02**, 063 (2018), arXiv:1711.09023.